Draft version April 27, 2009
Preprint typeset using LaTeX style emulateapj v. 10/09/06

arXiv:0904.4244v2 [astro-ph.CO] 27 Apr 2009

SPITZER OBSERVATIONS OF COLD DUST GALAXIES

C. N. A. Willmer[1], G. H. Rieke[1], Emeric Le Floc'h[2,3], J. L. Hinz[1], C. W. Engelbracht[1] Delphine Marcillac[4], and K. D. Gordon[5],

Draft version April 27, 2009

ABSTRACT

We combine new *Spitzer Space Telescope* observations in the mid- and far-infrared with SCUBA 850μm observations to improve the measurement of dust temperatures, masses and luminosities for 11 galaxies of the SCUBA Local Universe Galaxy Survey (SLUGS). By fitting dust models we measure typical dust masses of $10^{7.9}M_{\odot}$ and dust luminosities of $\sim 10^{10}L_{\odot}$, for galaxies with modest star formation rates. The data presented in this paper combined with previous observations show that cold dust is present in all types of spiral galaxies and is a major contributor to their total luminosity. Because of the lower dust temperature of the SCUBA sources measured in this paper, they have flatter Far-IR $\nu F_{\nu}(160\mu m)/\nu F_{\nu}(850\mu m)$ slopes than the larger *Spitzer Nearby Galaxies Survey* (SINGS), the sample that provides the best measurements of the dust properties of galaxies in the nearby universe. The new data presented here added to SINGS extend the parameter space that is well covered by local galaxies, providing a comprehensive set of templates that can be used to interpret the observations of nearby and distant galaxies.

Subject headings: Galaxies: fundamental parameters – galaxies: ISM – galaxies: photometry

1. INTRODUCTION

The mid and far infrared ($\sim$ 10-1000 μm) is a wavelength domain where some galaxy populations show significant changes over time (e.g., Puget et al. 1996; Sanders & Mirabel 1996; Chary & Elbaz 2001; Elbaz et al. 2002; Le Floc'h et al. 2005; Lagache, Dole & Puget 2005) and is therefore critical in our understanding of how galaxies form and evolve. The strong emission of galaxies in these wavelengths has been measured for objects with very different optical properties (spirals, ellipticals, Seyferts, interacting galaxies). The optical to IR ratio varies strongly from galaxy to galaxy and can be as low as few percent for the extreme IR galaxies ($L_{IR} > 10^{11}L_{\odot}$) where the IR emission dominates their total luminosity (Rieke & Lebofsky 1978).

This IR emission is mostly due to starlight absorbed by dust grains and re-emitted at longer wavelengths, though some objects have a significant non-thermal contribution coming from ionized gas in the interstellar medium (ISM) (Laurent et al. 2000a) and from active galactic nuclei and radio sources. The mid-IR light ($\lambda \sim$ 5–30 μm) is emitted by dust grains of different sizes (Désert, Boulanger & Puget 1990), that include very small grains (VSG), which are responsible for the thermal emission at 10-16 μm and are located in HII regions (Laurent et al. 2000b), and aromatic molecules (e.g., PAH, Leger & Puget 1984) that absorb ultra-violet photons generated in photo-dissociation regions (PDR) and re-emit in several bands between 3 and 17 μm (e.g., Laurent et al. 2000b; Lagache, Puget & Dole 2005). At longer wavelengths the emission is due to larger grains composed mainly of silicates (Désert et al. 1990). The latter absorb light from the ISM that is generated by young OB associations and from the old disk population (Lonsdale & Helou 1987). The ubiquity of dust in galaxies was demonstrated by the Infrared Astronomical Satellite (*IRAS*) survey, which covered over 90% of the sky in wavelengths ranging from 12 μm to 100 μm, and showed that most of the detected infrared luminosity could be explained by dust at temperatures of 40K and higher. However, evidence for dust at more than one temperature was first noted by Helou (1986) from the *IRAS* 12/25 μm to 60/100 μm color-color diagram which suggested that in addition to dust excited by the actively star forming regions, another component due to cooler "cirrus" was present and motivated the models proposed by Lonsdale & Helou (1987) mentioned above, and validated by Sauvage & Thuan (1992) in study comparing the Hα and far-IR luminosities. From the analysis of the gas to dust ratio in spiral galaxies, Devereux & Young (1990) could explain the observed discrepancy between the gas to dust ratios measured in external galaxies with the measurements obtained for the Galaxy by assuming the presence of a diffuse and cold (T < 30K) dust component dominant in the outer regions of galaxies, while the warmer dust would be predominant in the inner regions of the galaxy.

The detection of this cold dust required reaching longer wavelengths than accessible with *IRAS*. This became possible with the flight of the Infrared Space Observatory (ISO, Kessler et al. 1996) which allowed probing out to 200 μm and with the commissioning of the Submillimeter High Angular Resolution Camera (SHARC) at the Caltech Submilliter Observatory (e.g., Serabyn et al. 1999) and on the James Clerk Maxwell Telescope of the Submillimetre Common-User Bolometer Array (SCUBA) (Holland et al. 1999), observing at 850 μm.

The ISO observations of the nearby galaxies M 31

[1] Steward Observatory, University of Arizona, 933 North Cherry Avenue, Tucson, AZ 85721 ;cnaw@as.arizona.edu
[2] Spitzer Fellow
[2] Institute for Astronomy, University of Hawai'i 2680 Woodlawn Drive, Honolulu, HI 96822-1839
[4] Institut d'Astrophysique Spatiale, Bât. 121, Université de Paris Sud XI, 91405 Orsay Cedex, France
[5] Space Telescope Science Institute, 3700 San Martin Dr. Baltimore, MD 21218

TABLE 1
GALAXY SAMPLE

Galaxy	z	T	M_B	$\mathrm{Log}_{10}(L_{IR})$ $L_\odot$	$\mathrm{Log}_{10}(L_{TIR})$ $L_\odot$	SFR $M_\odot$ yr^{-1}
IC 797	0.00320	6	-16.81	9.27	8.81	0.2
IC 800	0.00779	5	-18.83	9.07	9.38	0.4
NGC 803	0.00703	5	-19.28	9.37	9.63	4.5
NGC 3270	0.02112	3	-21.22	10.23	10.56	2.0
NGC 4712	0.01473	4	-20.91	9.87	10.15	...
NGC 6137	0.03153	-5	-21.98	<9.94	<9.54	2.9
NGC 7047	0.01957	3	-20.50	9.98	10.35	3.5
NGC 7653	0.01433	3	-20.48	10.17	10.43	0.7
PGC 035952	0.01331	4	-19.73	9.61	9.80	1.0
UGC 10205	0.02211	1	-20.80	10.10	10.35	2.9
UGC 12519	0.01471	5	-19.76	9.95	10.30	2.7

Note. – Redshifts and morphologies come from the NASA Extragalactic Database (NED). The absolute magnitudes were derived from B magnitudes in NED. The L_{IR} measurements come from Vlahakis et al. (2005), while the L_{TIR} are derived from the the fits described in Section 3. The star formation rates are estimated following Bell (2003) and have estimated uncertainties $\sim 50\%$.

(Haas et al. 1998), M 33 (Hippelein et al. 2003) and M 101 (Tuffs & Gabriel 2003; Sauvage, Tuffs & Popescu 2005) and by Serabyn et al. (1999) for NGC 891 using SHARC, in wavelengths above 100 μm provided the first direct detections of cold dust. In a study of NGC 891, Popescu & Tuffs (2003) showed that the cold dust extends beyond the stellar disk, a similar behavior observed in HI disks, thus confirming the scenario proposed by Devereux & Young (1990). The data acquired for M 31 (Haas et al. 1998), M 101 (Tuffs & Gabriel 2003), M 33 (Haas et al. 1998; Hinz et al. 2004) and NGC 55 (Engelbracht et al. 2004) confirm that the cold and warm dust are distributed differently throughout the galaxy. In general, the warm dust component is easily identified in spiral arms and nuclei thanks to the larger density of star-forming regions, while the cold component is the source of the diffuse emission in the disk, though some localized components exist in the spiral arms (Tuffs & Popescu 2005).

The ground based observations using SCUBA to target nearby galaxies with *IRAS* detections also suggested the presence of significant amounts of cold dust. Dunne et al. (2000) obtained SCUBA observations for 104 galaxies and were able to obtain measurements of the local submillimeter and dust mass functions. However, because the original sample of Dunne et al. (2000) was selected on the basis of *IRAS* flux, they would preferentially detect galaxies with a significant amount of dust at T>40K. Based on the high gas-to-dust ratio (~ 600) compared to the Galactic value, Dunne et al. (2000) suggested that a cold dust component would be present in their sample, but which would not be directly detected by *IRAS*. To overcome the bias of using only *IRAS*-selected galaxies, Vlahakis, Dunne & Eales (2005) used the CfA1 redshift survey (Huchra et al. 1983) to define a sample to observe with SCUBA based exclusively on their optical properties. These were observed at 850 μm as part of the Scuba Local Universe Galaxy Survey (SLUGS). The SLUGS sample confirmed previous findings (e.g., Tuffs & Popescu 2003) using ISO that most of the dust mass is contained in cold particles. Whenever SCUBA data at 450 μm were available, supplementing the 850 μm and *IRAS* measurements, Vlahakis et al. (2005) found that two dust components (one warm, another cold) generally produced better fits to the observed distribution of Mid- to Far-IR fluxes. Their fits suggested that the total cold dust mass in these galaxies could be up to 100 times larger than the dust responsible for the emission at 5 μm through 70 μm.

Our understanding of dust properties of galaxies in the nearby universe has increased dramatically with the *Spitzer Nearby Galaxies Survey* (SINGS) key project (Kennicutt et al. 2003). SINGS has obtained extensive observations ranging from the far-UV observed with the Galaxy Evolution Explorer (GALEX, Martin et al. 2005) to the far-infrared for a representative sample of nearby galaxies comprising a wide range of luminosities, sizes and morphologies (e.g., Dale et al. 2005; Dale et al. 2007; Draine et al. 2007; Smith et al. 2007). These objects were pre-selected considering a parameter space defined by the optical morphology, the luminosity and the optical/FIR luminosity ratio (Kennicutt et al. 2003). Because prior to the launch of *Spitzer* most of the available mid- and far-IR measurements used to define the sample were obtained by *IRAS*, mainly sensitive to the emission by hot and warm dust, it is possible that galaxies with large amounts of cold dust are under-represented in SINGS. To test if this bias is present, we will use galaxies from SLUGS to address the far-IR properties of galaxies with a large cold dust component, and to provide a more complete view of the properties of galaxies over the whole extent of the IR wavelengths. In Section 2 we present the sample and describe the observations. In Section 3 we use modified black-body curves and dust models to estimate the temperatures of the dust components and characterize the Spectral Energy Distributions of these galaxies. Section 4 presents our conclusions. An H_0= 70 $kms^{-1}Mpc^{-1}$, $\Omega_m = 0.3$ and Ω_Λ=0.7 cosmology is assumed throughout.

2. DATA

2.1. *Sample definition*

The *Spitzer* observations targeted a subsample of 11 galaxies from Vlahakis et al. (2005) that have SCUBA observations in 850 μm (and in three cases additional data at 450 μm). The sample, presented in Table 1, contains galaxies with morphologies ranging from elliptical to late spiral, but with no cases of irregular or interacting

TABLE 2
Detector Parameters

Detector	λ_0 μm	Pixel Size arc sec	FWHM arc sec	Conversion Factor Jy/(MJy/Sr)	Calibration Uncertainty
IRAC 3.6	3.550	0.86	1.66	1.7492×10−5	1.8%
IRAC 4.5	4.493	0.86	1.72	1.7492×10−5	1.9%
IRAC 5.8	5.731	0.86	1.88	1.7492×10−5	2.0%
IRAC 8.0	7.872	0.86	1.98	1.7492×10−5	2.1%
MIPS 24	23.68	2.49	6.0	6.514×10−6	4%
MIPS 70	71.42	9.85	18	1.60	5%
MIPS 160	155.90	16	40	0.25	15%

galaxies. All galaxies in this sample are relatively quiescent in terms of their star formation activity with $\sim 2\ M_\odot$ yr^{-1}, estimated using the Bell (2003) relation. Because these galaxies are at moderately low redshift, with typical sizes of $\sim 2'$, the main subcomponents (bulge, disk, possibly spiral arms) are easily resolved in data ranging from the optical down to 24 μm.

2.2. *Observations*

The observations were taken as part of the *Spitzer* Guaranteed Time Observation Program 30348 (P.I.: G. H. Rieke) and used both the Infrared Array Camera (IRAC, Fazio et al. 2004), which is sensitive to the Rayleigh-Jeans stellar and warm dust emission, and the Mid Infrared Photometer for *Spitzer* (MIPS, Rieke et al. 2004), which is sensitive to warm dust in its bluer wavelength windows (24 μm and 70 μm) and cold dust at 160 μm.

The IRAC data were taken using all four wavelengths (3.6, 4.5, 5.8 and 8.0 μm), where a $5' \times 5'$ region of the sky was observed, using a 5 position dithered pattern, each exposed for 30 seconds, giving a total exposure of 150 seconds per band.

The MIPS observations were taken in photometry mode, where the spacecraft points at the object and then performs a series of mirror motions and spacecraft maneuvers to dither the source over the array (Rieke et al. 2004). All MIPS 24 μm observations were taken in a single cycle using a sequence of 12 dithers, followed by another series of 12 images which are offset to calculate the sky background. The total on-source integration is 120 seconds. Most 70 μm observations were also taken in a single cycle, though for two galaxies, because of their large apparent extent, "fixed cluster" observations using two cycles were necessary; the total integration time per pixel amounts to $\sim$ 125 seconds. In the case of 160 μm, the observations were taken over 4 cycles, which adds to a total integration time of $\sim$ 42 seconds per pixel.

Table 2 summarizes the instrumental parameters for each detector, consisting of the nominal wavelength (e.g., Reach et al. 2005; Rieke et al. 2008), the pixel size in the final mosaic, the FWHM of the point-spread function, the factor used to convert fluxes into Janskys and the calibration uncertainty.

2.2.1. *Data Reduction*

The pipeline-processed IRAC Basic Calibrated Data (BCD) were retrieved from the *Spitzer Science Center* (SSC) and were post-processed using the IRACproc suite of scripts (Schuster et al. 2006). These combine the SSC-processed images, reject outliers, correct for bad-pixels and cosmic rays, and produce the final flux-calibrated mosaic (Schuster et al. 2006), using the procedure and calibrations of Reach et al. (2005). The final photometry includes the calibration corrections determined by Rieke et al. (2008). The photometric uncertainties in the IRAC calibration are 1.8%, 1.9%, 2.0% and 2.1% for 3.6 μm, 4.5 μm, 5.8 μm and 8.0 μm respectively (Reach et al. 2005). The IRAC measurements already contain the corrections for extended sources[6]. No color corrections were applied to the tabulated data.

The MIPS data were reduced using the Data Analysis Tool version 3.06 (DAT) which is extensively described by Gordon et al. (2005). The DAT reads the raw data downloaded from the SSC archive, converts the integration ramps into slopes (in data numbers per second) removing at the same time instrumental effects, electronic non-linearities and stimulator flash latents in the case of 70 and 160 μm observations. The DAT also performs dark current, flat field and illumination corrections, removes distortions introduced by the off-axis location of the detectors, and creates a flux-calibrated mosaic (Gordon et al. 2005). The calibration of the MIPS data, described by Engelbracht et al. (2007), Gordon et al. (2007) and Stansberry et al. (2007), used repeated observations of stars which are referred to a model spectral energy distribution of an ideal A star ("Vega"), calibrated using the values in Rieke et al. (2008). The calibration uncertainties are $\sim$ 4% for 24 μm (Engelbracht et al. 2007), 5 % for 70 μm (Gordon et al. 2007) and $\sim$ 15 % for 160 μm (Stansberry et al. 2007).

2.2.2. *Photometry*

Galaxy fluxes were measured using the IRAF[7] *ellipse* task (Busko 1996), based on the method of Jedrzejewski (1987) to fit elliptical and circular isophotes. This task takes first guess values of object center, semi-major axis, position angle and ellipticity to calculate the ellipse at the starting radius. Excepting for the semi-major axis, the fitted parameters are used as input values for the next radius (outer or inner), which is calculated using a radial step set by the user. The *ellipse* task allows masking bad pixels as well as other objects in the image, such as foreground stars and background galaxies. Since *ellipse* does not calculate sky background values, these

[6] `http://ssc.spitzer.caltech.edu/irac/calib/extcal/index.html`
[7] IRAF is distributed by the National Optical Astronomy Observatory, which is operated by the Association of Universities for Research in Astronomy (AURA), Inc., under cooperative agreement with the National Science Foundation.

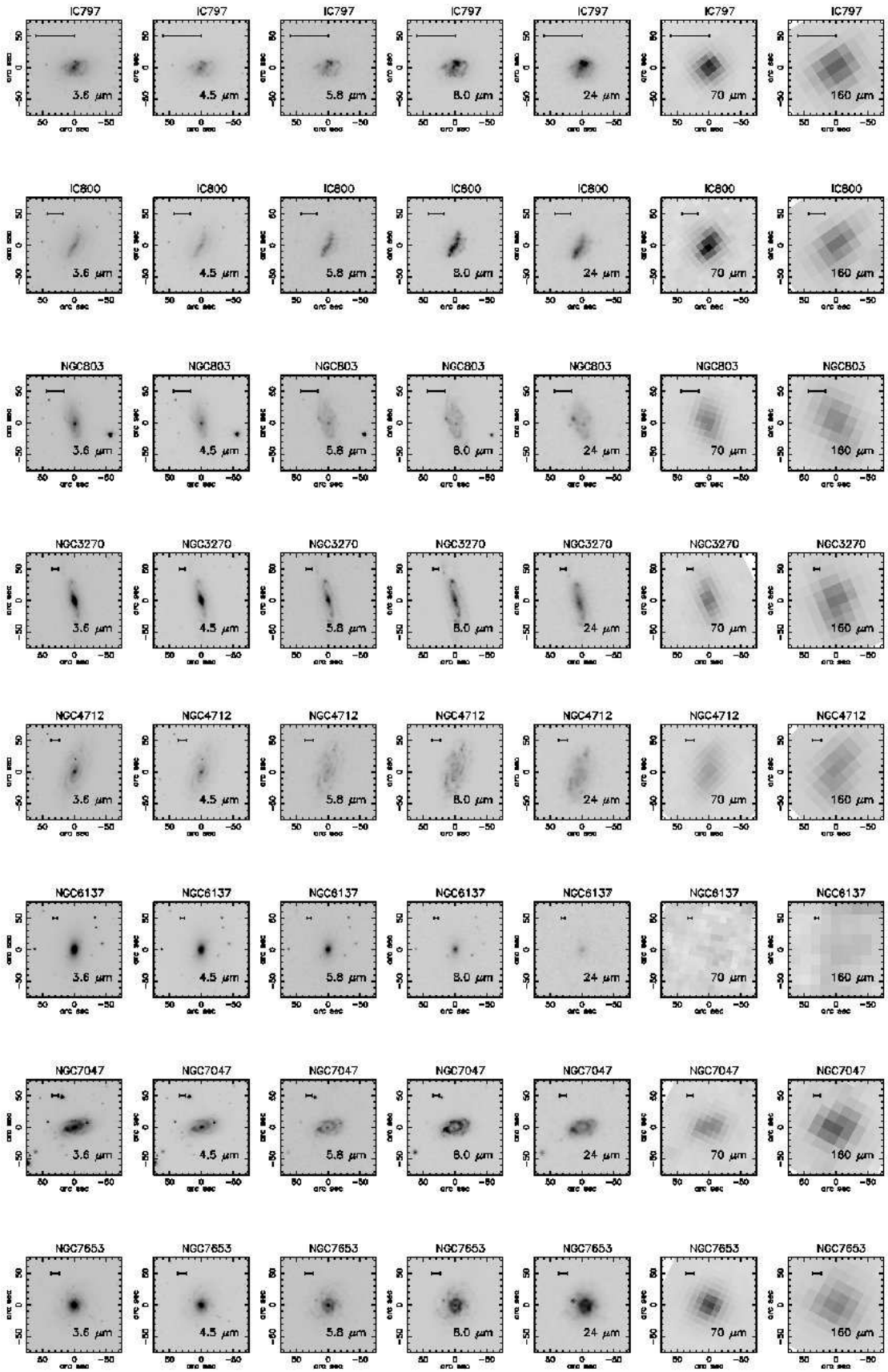

FIG. 1.— Postage stamp images of galaxies in this sample. The galaxy identification is noted at top of window, while the band is noted in the lower right corner. A scale bar corresponding to 2 kpc at the galaxy distance is shown in the upper left corner of each figure.

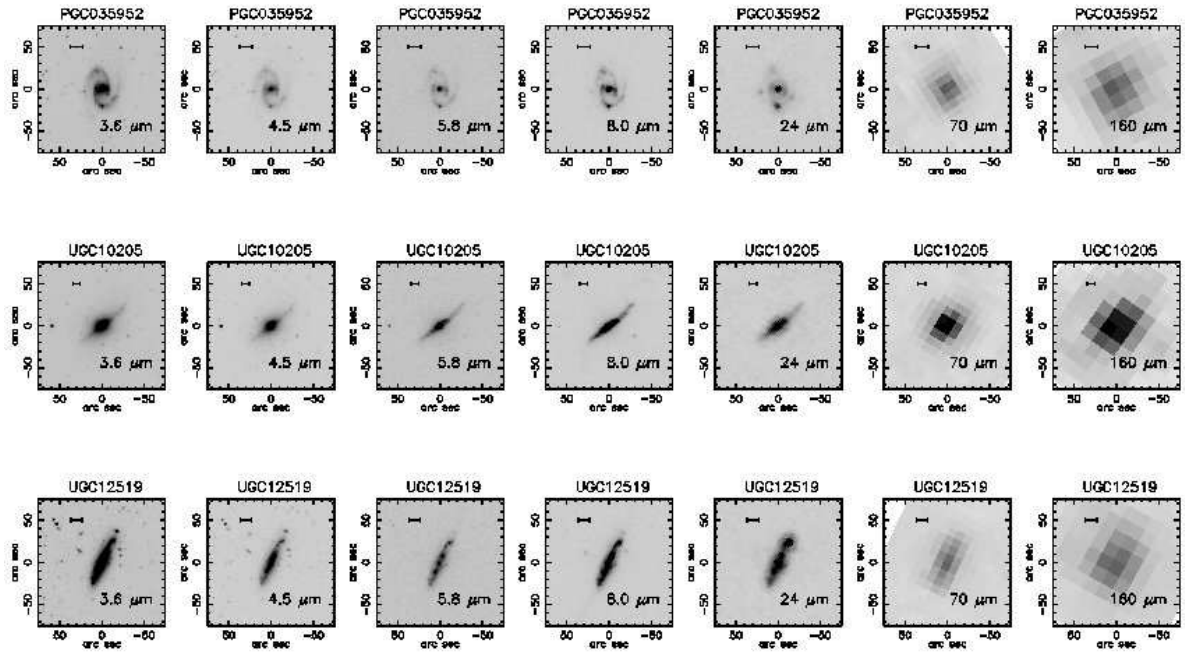

FIG. 1.— (cont.)

TABLE 3
GALAXY SAMPLE: *Spitzer* MEASUREMENTS

Name	3.6μm Jy	4.5μm Jy	5.8μm Jy	8.0μm Jy	24μm Jy	70μm Jy	160μm Jy
IC 797	0.021± 0.003	0.014± 0.002	0.027± 0.004	0.065± 0.010	0.072± 0.007	0.939± 0.188	2.708± 0.677
IC 800	0.017± 0.003	0.012± 0.002	0.020± 0.003	0.042± 0.006	0.046± 0.005	0.519± 0.104	1.463± 0.366
NGC 803	0.045± 0.007	0.029± 0.004	0.042± 0.006	0.092± 0.014	0.071± 0.007	0.904± 0.181	4.241± 1.060
NGC 3270	0.050± 0.007	0.031± 0.005	0.043± 0.006	0.103± 0.015	0.083± 0.008	0.725± 0.145	3.727± 0.932
NGC 4712	0.028± 0.004	0.019± 0.003	0.027± 0.004	0.071± 0.011	0.069± 0.007	0.711± 0.142	3.236± 0.809
NGC 6137	0.058± 0.009	0.036± 0.005	0.022± 0.003	0.018± 0.003	0.007± 0.001	0.017± 0.003	0.030± 0.007
NGC 7047	0.028± 0.004	0.019± 0.003	0.031± 0.005	0.067± 0.010	0.060± 0.006	0.722± 0.144	2.201± 0.550
NGC 7653	0.046± 0.007	0.030± 0.005	0.060± 0.009	0.145± 0.022	0.131± 0.013	1.776± 0.355	4.346± 1.087
PGC 035952	0.011± 0.002	0.006± 0.001	0.011± 0.002	0.028± 0.004	0.045± 0.005	0.611± 0.122	1.211± 0.303
UGC 10205	0.042± 0.006	0.028± 0.004	0.029± 0.004	0.056± 0.008	0.041± 0.004	0.727± 0.145	1.762± 0.441
UGC 12519	0.020± 0.003	0.013± 0.002	0.033± 0.005	0.078± 0.012	0.108± 0.011	1.081± 0.216	3.690± 0.922

TABLE 4
GALAXY SAMPLE: MEASURES FROM THE LITERATURE

Name	J mag	H mag	K mag	12μm Jy	60μm Jy	100μm Jy	450μm Jy	850μm Jy
IC 797	11.58±0.04	11.07±0.06	10.80±0.07	0.200± 0.043	0.730± 0.045	2.110± 0.130	...	0.085±0.021
IC 800	11.19±0.03	11.34±0.03	10.58±0.06	0.130± 0.038	0.600± 0.056	1.560± 0.271	...	0.076±0.019
NGC 803	10.71±0.02	10.01±0.03	9.83±0.04	0.140± 0.040	0.730± 0.047	2.850± 0.134	0.631±0.22085	0.093±0.019
NGC 3270	10.76±0.02	10.06±0.01	9.73±0.02	0.130± 0.032	0.620± 0.040	2.280± 0.107	...	0.059±0.014
NGC 4712	10.92±0.04	10.42±0.05	10.09±0.05	0.070± 0.033	0.500± 0.044	1.880± 0.113	...	0.102±0.023
NGC 6137	10.51±0.02	9.81±0.02	9.55±0.03	0.020± 0.020	0.100± 0.100	0.380± 0.380	...	0.029±0.010
NGC 7047	11.13±0.03	10.47±0.04	10.20±0.05	0.120± 0.025	0.580± 0.059	2.110± 0.251	...	0.055±0.013
NGC 7653	10.71±0.02	10.03±0.02	9.75±0.04	0.280± 0.041	1.440± 0.065	5.460± 0.434	...	0.112±0.020
PGC 035952	12.26±0.05	11.58±0.07	11.29±0.07	0.030± 0.034	0.420± 0.047	1.600± 0.212	0.421±0.14735	0.051±0.013
UGC 10205	10.87±0.02	10.14±0.02	9.89±0.03	0.060± 0.041	0.460± 0.056	1.560± 0.192	...	0.058±0.015
UGC 12519	11.62±0.03	10.89±0.03	10.61±0.06	0.130± 0.034	0.960± 0.052	3.280± 0.321	0.408±0.1428	0.074±0.016

Note. – J, H and K magnitudes come from the 2MASS archive at `http://irsa.ipac.caltech.edu/`; the *IRAS* measurements were obtained using the Scanpi tool at `http://scanpiops.ipac.caltech.edu:9000/applications/Scanpi/index.html`. The 450 and 850 μm measurements come from Vlahakis et al. (2005)

must be subtracted prior to fitting the ellipses.

For the IRAC data, the initial parameters were obtained from the Bertin & Arnouts (1995) source extractor (SExtractor) catalog derived for each image, while the segmentation image produced by SExtractor was used to mask out stars and background galaxies. To produce a valid "data quality file" input to *ellipse* all pixels belonging to the object and the sky were set to zero in this image. In addition to masking foreground and background sources, the "data quality file" is also used to flag pixels affected by instrumental defects and cosmic rays. The same procedure to mask background/foreground objects was used for the MIPS observations. In the case of MIPS 160 μm images, gaps in the sky that were not covered by the array were masked out by hand.

Prior to the photometry, fluxes were converted from MJy/Sr into Janskys using the factors presented in Table 2, which depend on the pixel size. The sky level in the IRAC images was determined by fitting a low order polynomial in regions more than 100″ away from the galaxies, which was then subtracted from the image. For MIPS images the background sky was estimated using several boxes of 25 pixels from which a mean sky value was determined and subtracted. For most galaxies the surface brightness profile flattens at large radii, demonstrating that the sky subtraction was effective. However, in a few cases, in particular for 160 μm, the presence of residual sky (caused by the foreground Galactic Cirrus) can affect the final measurements of galaxies with very low flux in this band. The circular and elliptical isophotes were fit to distances of ~ 100 ″ from the center and for most bands convergence was reached at about 50″. For most of the sources considered in this work, the results derived from elliptical and circular apertures differ by less than the estimated uncertainties. Based on this, the circular aperture photometry was adopted for the final flux measurements, which are presented in Table 3.

2.3. *Archival data of other wavelengths*

The *Spitzer* IRAC and MIPS data are supplemented in this paper with published data, presented in Table 4, consisting of the 2MASS photometry in the near- infrared, the sub-mm measurements by Vlahakis et al. (2005) and *IRAS* archival data.

The 2MASS (Jarrett et al. 2000) near-Infrared magnitudes were obtained from the NASA Extragalactic Database (NED). The 2MASS measurements are the total magnitudes measured by extrapolating the near-IR surface brightness to a diameter corresponding to roughly 4 disk scale lengths defined from the J-band image due to its greater sensitivity at lower surface brightnesses (Cutri et al. 2006). Because most of the galaxies presented in this work are relatively bright, the typical uncertainties in the photometry are $\sim 3\%$. Because of the bright apparent magnitudes of these galaxies, the loss of light coming from low surface brightness regions must be comparable to that found by Bell et al. (2003) for K$\sim$13.5 galaxies, which is ~ 0.1 magnitudes, and should not affect our conclusions.

The sub-mm data were presented by Vlahakis et al. (2005). The 850 μm fluxes were measured from the SCUBA maps choosing an aperture that would optimize the signal to noise ratio, taking into account the optical extent of the galaxies indicated by the Digitized Sky Survey[8].

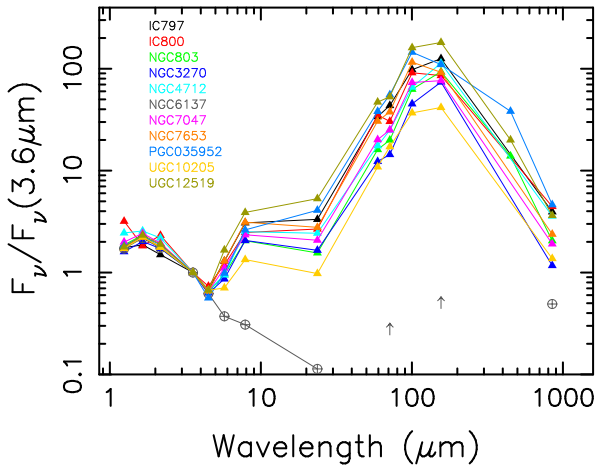

FIG. 2.— Spectral energy distribution for the ensemble of SLUGS galaxies observed for this project, normalized at 3.6 μm. The stellar component shows little variation, while all galaxies, with the exception of NGC 6137 show a bump in the mid-IR due to the aromatic features, followed by a strong peak in the far-IR caused by the presence of cold dust. For NGC 6137 the *Spitzer* measurements at 70 and 160 μm are only upper limits. The combined 24 and 850 μm data points are suggestive of a power-law emission in the mid- and far-IR for this galaxy.

The *IRAS* fluxes were obtained by co-adding images using the NASA/IPAC Infrared Science Archive's IRAS Scan Processing and Integration (SCANPI) tool and selecting the Noise-Weighted Mean. Given the much higher quality of the 24 μm fluxes from MIPS, we will not use the *IRAS* 25 μm fluxes in the analyses that follow.

3. ANALYSIS

Figure 1 presents a mosaic of all images taken with IRAC and MIPS for the SLUGS galaxies observed with *Spitzer*. The images are ordered in observed wavelength and the scale bar in each panel represents a projected angular distance of 2 kpc. All galaxies are resolved in the IRAC bands, and different subcomponents of galaxies are easily identified. Similar to the SINGS galaxies (Dale et al. 2005) and the galaxies of Hinz et al. (2006, 2007), the older stellar populations provide the main contribution in bluer IRAC bands (3.6 and 4.5 μm) while the dustier disk becomes more prominent in the redder 5.8 and 8.0 μm bands. Although most galaxies of this sample are resolved in the MIPS bands, galaxy subcomponents are only easily identified in the MIPS 24 μm images. While the galaxy outlines and most prominent components can be seen in the 70μm images, the 160 μm observations in general show very little detail, though the extent to which the emission is seen is comparable to that of the stellar component. One galaxy (NGC 6137) is only weakly detected at 70 and 160 μm and shows a point-like source at 24 μm, probably due to the radio source at the center of this galaxy (Giovanini et al. 2005). The new data suggest that probably all, rather than $\sim 20\%$, of the 850

[8] The Digitized Sky Surveys were produced at the Space Telescope Science Institute under U.S. Government grant NAGW-2166. The images of these surveys are based on photographic data obtained using the Oschin Schmidt Telescope on Palomar Mountain and the UK Schmidt Telescope. The plates were processed into the present compressed digital form with the permission of these institutions.

μm emission detected by Vlahakis et al. (2005) for this galaxy is due to an active nucleus.

The spectral energy distribution of the SLUGS galaxies normalized at 3.6 μm, where the galaxy light is dominated by old stellar populations, is shown in Figure 2. Each galaxy is represented by a different color as noted in the key. Most objects show similar spectral shapes, with intensities peaking at ~ 100 μm. The only exception is NGC 6137.

3.1. *Dust component temperatures*

The new MIPS data combined with existing *IRAS* and SCUBA measurements can be used to estimate the dust component temperatures and masses using composite grey-body curves (e.g., Vlahakis et al. 2005). For two components these are:

$$F_\nu = A_w \nu^\beta B_\nu(\frac{\nu}{1+z}, T_w) + A_c \nu^\beta B_\nu(\frac{\nu}{1+z}, T_c) \quad (1)$$

where A_w and A_c are the relative contributions due to the warm and cold dust components. The masses can be estimated from (Vlahakis et al. 2005):

$$M = \frac{F_\nu D^2}{k_d} \left[\frac{A_w}{B_\nu(\frac{\nu}{1+z}, T_w)} + \frac{A_c}{B_\nu(\frac{\nu}{1+z}, T_c)} \right] \frac{1}{A_w + A_c}, \quad (2)$$

where $k_d = 0.07 \pm 0.02$ m^2 kg^{-1} is the average dust mass opacity measured at 850 μm by James et al. (2002), D is the galaxy distance and B_ν the modified Planck function. Since the average radiation field combines emission at several intensity levels (e.g., Draine & Li 2007; Draine et al. 2007; see below), the temperatures should only be taken as a rough estimate of the "effective dust temperature" (Blain et al. 2004). The fits were calculated considering three values for the dust emissivity index (β = 1.0, 1.5, 2.0), $\beta = 2.0$ producing better constrained fits. This is also the value of β used by Vlahakis et al. (2005) in their analysis. The fits are presented in Figure 3, while Table 5 lists the temperatures and errors for the cold and warm components, and the estimated mass ratio between warm and cold components. The larger wavelength range of the present sample allows more constrained fits than was possible for Vlahakis et al. (2005). For the 3 objects in common for which they calculate two-component fits, the most dramatic difference is found for UGC 12519, where the measurements change from (T_w, T_c, M_{cold}/M_{warm}) = (28, 18, 12) to (56.0, 19.6, 1054). For NGC 803 Vlahakis et al. (2005) find two possible solutions (33, 18, 92) and (60, 19, 2597). The latter is closer to the values measured here (54.7, 28.4, 1812). For PGC 35952 the *IRAS*+SCUBA measurements produce (58, 18, 1859), while we find (54.7, 19.0,1054). The temperatures agree within the estimated errors, though the dust mass ratios can differ significantly. As noted by Draine et al. (2007) even small shifts in temperatures imply very large changes in the dust masses, as seen in this comparison. Because of the paucity of data longwards of 160 μm for the SLUGS sample analysed here (only 3 galaxies have 450 μm data) we cannot test for the existence or absence of dust colder than 18 K which has been found in low-metallicity dwarf galaxies (e.g. Galliano et al. 2005).

3.2. *Galaxy models*

More robust estimates of the (total) dust masses can be obtained using models with a more complex dust composition (e.g., Désert et al. 1990; Guiderdoni et al. 1998; Dale et al. 2001; Dale & Helou 2002; Marshall et al. 2006; Siebenmorgen & Krügel 2007; Draine & Li, 2007; Draine et al. 2007). These models, combined with the empirical SEDs constructed using existing observations (e.g., Chary & Elbaz 2001; Lagache et al. 2003; Lagache et al. 2004; Rieke et al. 2009) have been used to explain the strong evolution as a function of redshift in number and density that is observed in the mid and far infrared (e.g., Puget et al. 1995; Le Floc'h et al. 2005; Pérez-González et al. 2008). Typically the models describe the mid- and far-IR properties of galaxies combining the UV output from hot young stars, which is re-radiated by small size particles, and larger grains that are heated stochastically or are in thermal equilibrium (Désert, Boulanger & Puget 1990).

To analyse the sample presented in this paper and compare their properties with those measured for SINGS galaxies, we follow the analysis of Draine et al. (2007), by using the models calculated by Draine & Li (2007). The latter work builds upon many previous papers by Draine and collaborators (e.g., Li & Draine 2001; Weingartner & Draine 2001a; 2001b) by taking into account the results of recent observations (e.g., Smith et al. 2007). These models are based on a series of physically motivated assumptions, and can be used to estimate the galaxies' total dust masses. The dust models are parameterized both by the dust composition and by the stellar radiation field incident on the dust grains. In the Draine et al. (2007) models, most of the dust is assumed to be located in a diffuse ISM that is heated by a general interstellar radiation field (e.g., Lonsdale & Helou 1987) typical of normal spiral galaxies (U_{min}). This field has an equilibrium temperature ~ 16.2 K (based on Milky Way measurements by Finkebeiner, Davis & Schlegel 1999) while a range of radiation field intensities heats the dust particles to different temperatures. The fraction of galaxy dust that is subject to the intense radiation field generated by hot young stars (U_{max}) is denoted by γ and is quantified as a percentage of the total dust emission of the galaxy. The emission at $\lambda < 20$ μm (Draine & Li 2007) is mainly due to aromatic grains, whose contribution is characterized by the q_{PAH} parameter, which quantifies the ratio between the mass in aromatic grains containing less than 1000 carbon atoms and the total dust mass. Weingartner & Draine (2001) calculated several models that use different grain size distributions and with different q_{PAH} values, but are constrained to follow the average ISM extinction law, reproducing the Milky Way's wavelength-dependent extinction curves (Draine & Li 2007). The models, described in Table 3 of Draine et al. (2007), show slight variations in the total dust mass to hydrogen ratio but have values of $M_{dust}/M_H \sim 0.01$, slightly higher than the prefered value of Draine et al. (2007) of 0.0073, calculated assuming an approximately solar metallicity for the Galaxy's ISM. The stellar continuum for wavelengths greater than 5 μm is well described by a 5000 K black-body (e.g., Smith et al. 2007; Draine et al. 2007). Following Draine et al. (2007) the SEDs of

TABLE 5
Temperature fit parameters for SLUGS and SINGS galaxies

Galaxy	T_{warm} K	T_{cold} K	M_{cold}/M_{warm}
IC 797	53.9± 1.3	18.1± 1.0	1213
IC 800	51.1± 2.8	16.2± 2.8	1065
NGC 3270	56.9± 1.9	18.5± 0.9	1918
NGC 4712	56.2± 0.9	17.0± 0.4	3213
NGC 7047	54.5± 2.8	18.8± 1.4	1248
NGC 7653	54.7± 4.0	19.9± 2.1	1008
NGC 803	54.7± 1.0	18.4± 0.4	1812
PGC 035952	54.7± 4.4	19.0± 2.5	1054
UGC 10205	52.5± 2.8	18.4± 1.8	1098
UGC 12519	56.0± 2.1	19.6± 1.0	1054
NGC 337	52.8± 3.2	20.6± 3.8	337
NGC 1482	56.1± 3.6	23.5± 5.2	109
NGC 2798	58.0± 4.3	24.4± 5.4	116
NGC 2976	54.9± 3.7	19.1± 5.1	800
NGC 3190	54.2± 3.4	19.9± 3.9	766
Mrk 33	60.7± 5.1	24.3± 7.2	111
NGC 3521	55.2± 2.9	18.5± 3.8	985
NGC 3627	55.2± 3.0	19.2± 4.6	571
NGC 4536	55.5± 2.9	20.6± 4.6	225
NGC 4569	58.4± 3.4	19.7± 2.9	973
NGC 4631	52.6± 3.4	18.9± 4.0	539
NGC 4826	52.4± 3.8	20.3± 5.0	362
NGC 5195	59.4±27.9	25.7± 9.5	258
NGC 5713	54.9± 2.9	20.2± 4.1	307
NGC 5866	57.2±16.1	24.5± 3.1	878
NGC 7331	54.4± 3.2	19.4± 2.8	660

TABLE 6
Results using Draine & Li dust models fitting U_{max}

Galaxy	M_{dust} $M_\odot$	L_{dust} $L_\odot$	γ %	<U>	q_{PAH} %	U_{max}
IC 797	6.71	8.85	7.11	1.01	4.58	10^3
IC 800	7.51	9.44	15.55	0.63	3.90	10^3
NGC 3270	8.33	10.57	0.55	1.28	4.58	10^6
NGC 4712	8.14	10.17	1.20	0.79	3.90	10^5
NGC 7047	8.00	10.37	1.94	1.73	4.58	10^4
NGC 7653	8.05	10.45	4.55	1.88	4.58	10^3
NGC 803	7.43	9.64	0.00	1.20	4.58	10^6
PGC 035952	7.77	9.85	8.57	0.88	2.50	10^4
UGC 10205	8.18	10.38	7.33	1.16	3.90	10^3
UGC 12519	7.95	10.31	1.10	1.71	3.90	10^6

TABLE 7
Results using Draine & Li dust models with fixed U_{max}=10^6

Galaxy	M_{dust} $M_\odot$	L_{dust} $L_\odot$	γ %	<U>	q_{PAH} %
IC 797	6.57	8.82	0.74	1.31	4.58
IC 800	7.05	9.40	0.73	1.64	4.58
NGC 3270	8.33	10.57	0.55	1.28	4.58
NGC 4712	8.14	10.17	0.82	0.78	3.90
NGC 7047	8.02	10.36	0.65	1.62	4.58
NGC 7653	7.98	10.44	0.49	2.12	4.58
NGC 803	7.43	9.64	0.00	1.20	4.58
PGC 035952	7.51	9.81	1.86	1.48	2.50
UGC 10205	7.91	10.36	0.18	2.04	4.58
UGC 12519	7.95	10.31	1.10	1.71	3.90

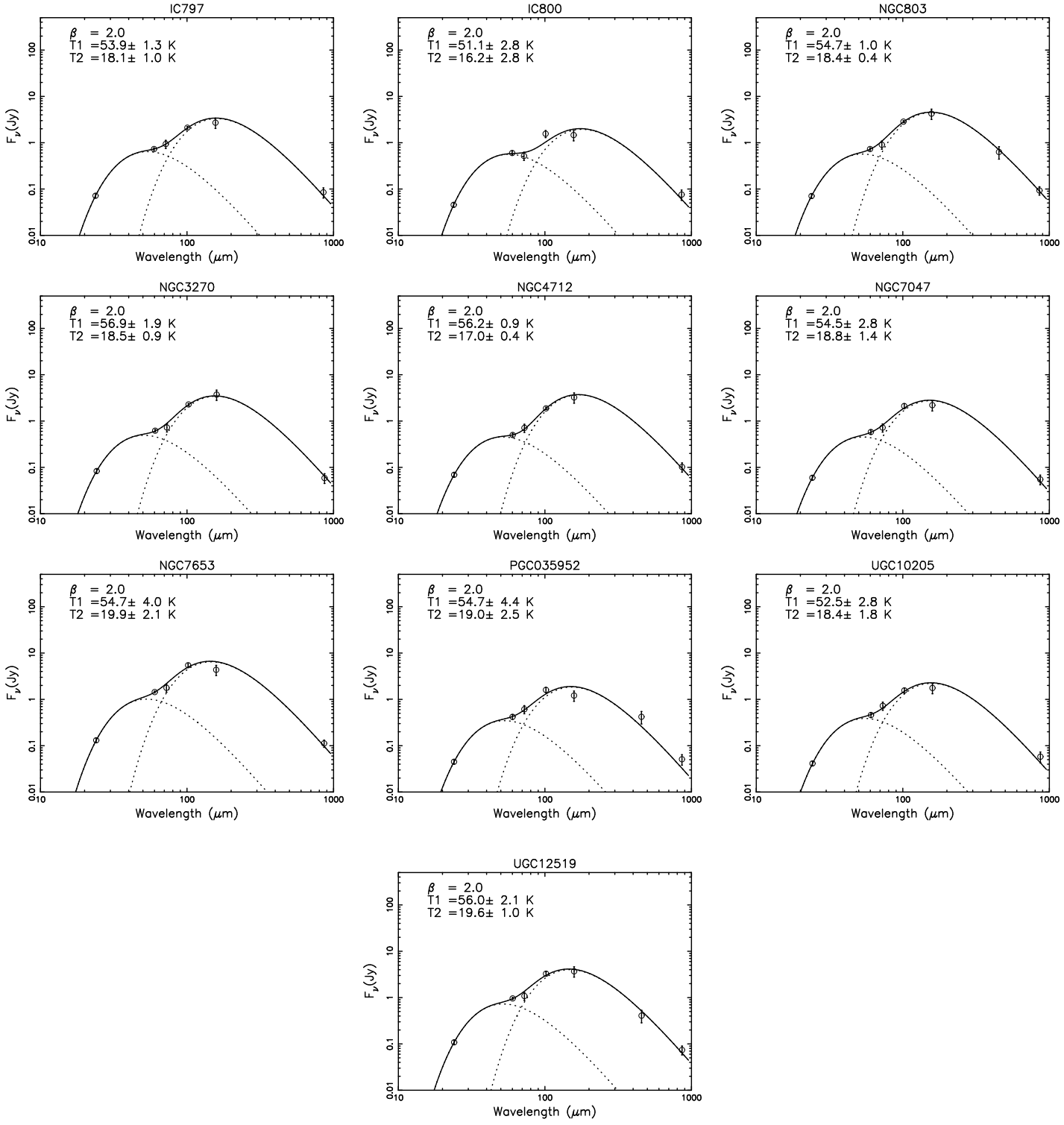

FIG. 3.— Temperature fits using modified blackbody curves with the emissivity index β=2, assuming two temperature components. The dotted curves represent the individual components, the solid curve the combined flux. The values of best fit temperatures and associated errors are also shown in the figure.

SLUGS galaxies are fit by minimizing

$$\chi^2 = \sum_{i=1}^{N_{bands}} \frac{(f_{obs}(\nu_i) - F_{model}(\nu_i))^2}{err^2_{obs} + err^2_{model}}. \quad (3)$$

where, using the Draine et al. (2007) notation, the observed flux is a combination of the stellar component with the emission due to the diffuse ISM and dust heated by hot stars:

$$F_{model}\ (\nu_i) = \Omega_* B_\nu(T_*, \nu_i) + \frac{M_{dust}}{4\pi D^2} \times \left[(1-\gamma)p^0_\nu(j_m, U_{min}) + \gamma p_\nu(j_m, U_{min}, U_{max}, \alpha)\right]; \quad (4)$$

p^0_ν and p_ν represent the power radiated by the dust mixture per unit mass and frequency that is subject to radiation field intensity of U_{min} (p^0_ν) or to a range of intensities (p_ν), assumed to follow a power-law characterized by the exponent α (Draine et al. 2007). Following these authors, we adopt α=2. The models for the PAH abundance, the radiation field, the total M_{dust}/M_H ratio and the extinction are combined into j_m, the specific power radiated per unit dust mass[6].

When calculating the fits, we first normalize the stellar component (Ω_*) using the 2MASS photometry in J and H. This is followed by the calculation of the dust model normalization; final fits are obtained by varying γ and looping through all models sharing the same proportion of aromatic masses (q_{PAH}) and general radiation field (U_{min}). The results of this procedure are presented in Table 6, while Figure 4 shows the measured SEDs and the best fitting model. Also shown in Fig. 4 are the graphic estimates of the stellar flux, the flux due to dust in photo-dissociation regions and the flux emitted by dust in "the diffuse ISM heated by a single radiation field" (Draine et al. 2007). Most galaxies are reasonably well fit by the cold temperature diffuse component with a small contribution from hot dust in photo-dissociation regions (PDR). In the case of NGC 803 the fits are consistent with no presence of PDRs, though the IRAC data do not show any gross inconsistency with the presence of aromatic emission, which is generally produced in regions with strong UV emission. The analysis by Bendo et al. (2008) of the correlation observed between the aromatic emission at 8 μm and 160 μm in a sample of nearby spiral galaxies as well as that of Haas, Klaas & Bianchi (2002) shows that such emission is expected. No fits are presented for NGC6137 because its FIR spectrum is probably dominated by non-thermal emission. The results in Table 6 also fit for U_{max}, which represents the upper cut off of the stellar intensity field (Draine et al. 2007). Fixing the value of $U_{max} = 10^6$ produces the fits presented in Table 7. When fitting for U_{max} we find that the residuals in the far-IR are slightly smaller.

3.3. *Comparison with SINGS*

3.3.1. *Sample biases*

The combination of selection criteria (in addition to the small sample sizes of SLUGS and SINGS), imposes a major limitation on the possible analyses with these samples. As described by Vlahakis et al. (2005), the parent sample for SLUGS is defined from the CfA1 Redshift Survey (Huchra et al. 1983), which in principle should be unbiased as far as the cold-dust properties of galaxies are concerned (cf.,Section 1). The SLUGS galaxies selected for *Spitzer* observations are a subset of this larger sample.

The optical SLUGS sample was defined considering the number of objects within a well defined region of the sky and with an angular size that would fit inside the SCUBA field of view. The parent sample contains a total of 97 galaxies, observations having been taken for 81. Of the latter, 52 were detected in 850 μm, while 29 (36%) only provided upper limits. Early type (E+S0) galaxies comprise 14 (48 %) of the non-detections (corresponding to 17% of the total observed sample), spirals 8 (28%) and the remainder are either multiple systems or compact sources. The sample observed with *Spitzer* contains 10 spiral galaxies and 1 elliptical, which is close to the morphological mix of the SLUGS observed sample. Thus the small proportion of early-types in the *Spitzer* sample reflects in part the low detection rate of these galaxies in the SLUGS sample (Vlahakis et al. 2005). There is a risk that the SLUGS/*Spitzer* sample is not representative of cold-dust properties of the local population of galaxies, being biased towards galaxies with larger cold dust masses.

In a similar way, SINGS galaxies by design were not chosen to represent a volume-limited sample of galaxies but rather to be representative of the local morphology, luminosity and L_{FIR}/L_B parameter space (Kennicutt et al. 2003). Thus, when interpreting the comparisons that follow one must take into account that neither sample is a "fair" representation of the local mix of galaxy properties, so that the results may not be valid for the general galaxy distribution. In particular, the observations of SINGS galaxies with SCUBA did not follow any type of preselection based on their dust properties. Of the 26 SINGS galaxies with SCUBA data, 13 were observed after the SINGS sample was defined, while data for the remainder were taken from the SCUBA archive by Dale et al. (2005). However, we should note that Draine et al. (2007) identify 9 objects which have lower confidence SCUBA observations which are galaxies for which the data reduction removes extended emission (4 galaxies); galaxies for which SCUBA measurements do not cover the total spatial extent where emission in 160 μm is detected (4 galaxies) and one galaxy for which the 850 μm emission is dominated by an AGN.

3.3.2. *Comparison between SINGS and SLUGS*

One motivation for the new *Spitzer* observations in this work was the significantly different distribution observed using the sample of SLUGS galaxies relative to SINGS when considering the *IRAS* 25 to 60 μm and 100 to 850 μm color-color distribution, which measures the relative intensity of warm to cold dust emission. Figure 5 shows the analogous distribution using MIPS data for both samples in the 24 to 70 μm and 160 to 850 μm colors, where it is clearly seen that SLUGS (solid circles) and SINGS galaxies *with* SCUBA measurements (diamonds) occupy mainly different regions (we should note that the parent SLUGS sample covers the entire *IRAS* 25 to 60 μm color range). Even when including SINGS galaxies for which the 850 μm may

[6] Tables with j_m values are available at the `ftp://ftp.astro.princeton.edu/draine/dust/irem4/` site.

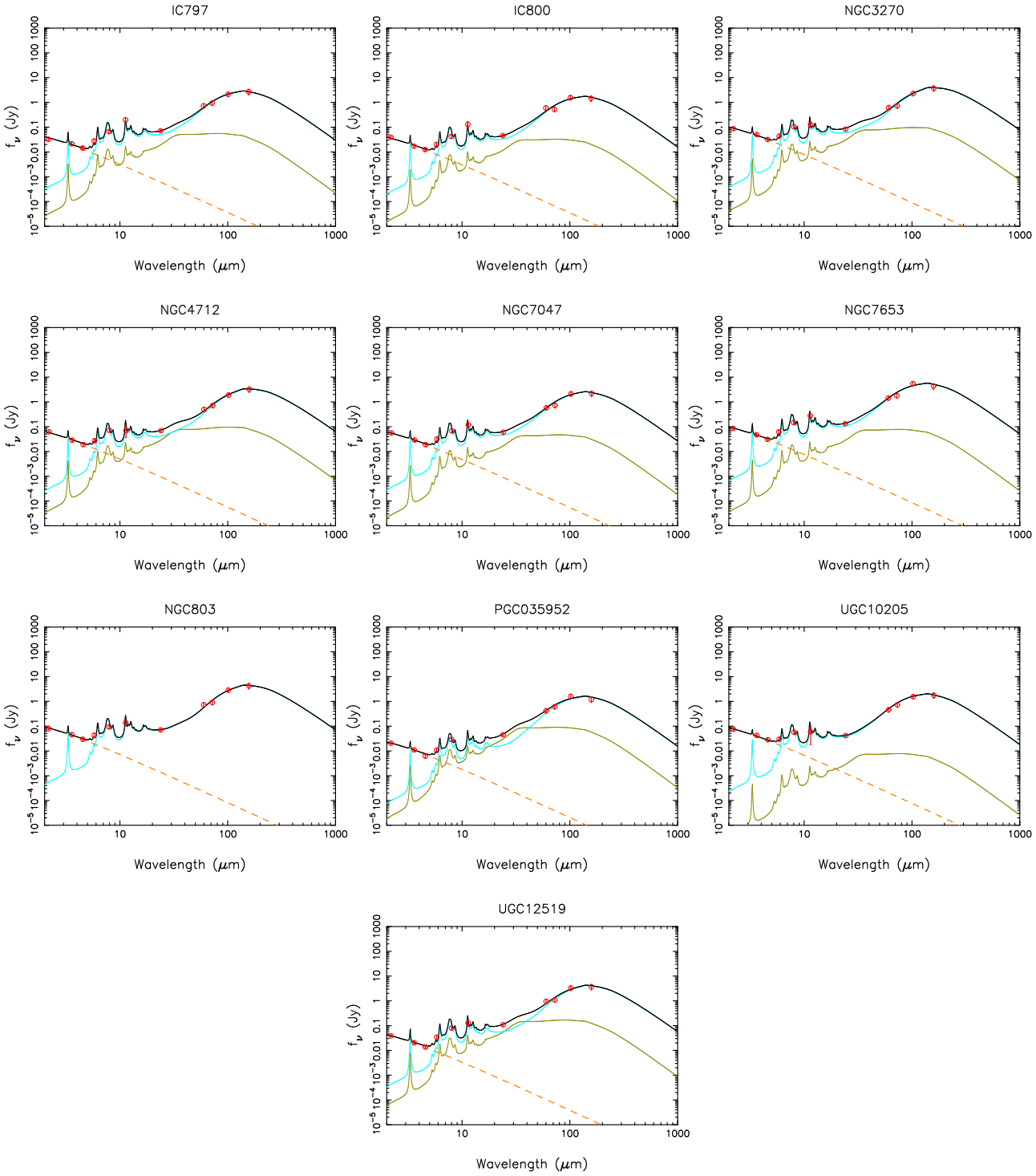

FIG. 4.— Spectral energy distribution of SLUGS galaxies including data from 2MASS, *IRAS*, SCUBA, IRAC and MIPS observations (open circles). The (estimated) error bars for most measurements are smaller than data points for most of the IRAC and MIPS data. Colors represent fits using the Draine & Li (2007) models; the dashed orange line represents the estimated stellar flux, the green line the emission due to grains heated in photo-dissociation regions, cyan the emission from dust due to a single radiation field. The black line represents the sum of these components. The parameters for these fits, which also fit for U_{max} the maximum starlight intensity, are presented in Table 6.

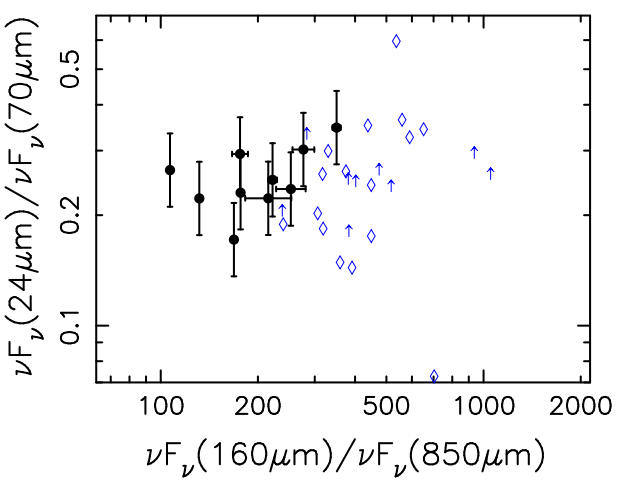

FIG. 5.— Color-color distribution for galaxies with SCUBA measurements. SLUGS galaxies are represented by black solid circles while the diamonds denote SINGS galaxies with good SCUBA measurements. The arrows represent upper limits of the νFν(160μm)/νFν(850μm) ratio of galaxies for which the SCUBA measurements are probably underestimated (Draine et al. 2007). The segregation between both samples is very clear. While both sample show a similar behavior in the 24/70 μm color which measures the mid-IR slope, the SLUGS galaxies show flatter 160/850 μm slopes due to the larger contribution due to cold dust.

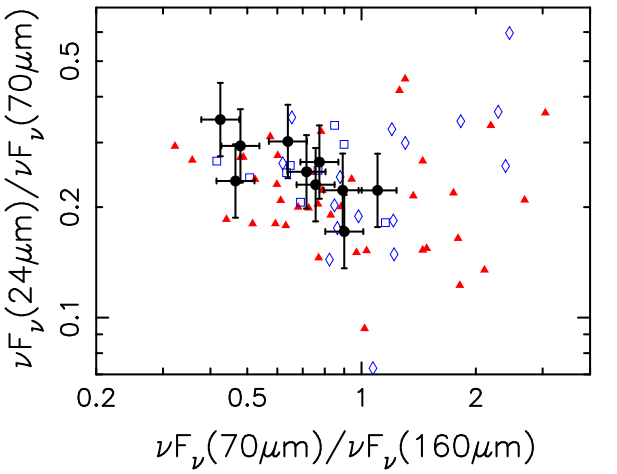

FIG. 6.— Color-color distribution following Draine et al. (2007) of SLUGS galaxies (black circles) compared to SINGS galaxies with good SCUBA (diamonds) and lower confidence (suares) detections, and without (triangles). The location of SLUGS galaxies towards lower values of $(\nu F_\nu)_{70\mu m}/(\nu F_\nu)_{160\mu m}$ is expected for galaxies with significant amounts of cold dust (Draine et al. 2007).

be underestimated, thus providing upper limits to the νF$_\nu$(160μm)/νF$_\nu$(850μm) ratio (noted by the arrows), the locus of SLUGS galaxies still differs from that of the increased sample.

We now consider several combinations of measureable parameters to examine whether this difference found between SLUGS and the SINGS subsample with SCUBA data also extends to full SINGS sample when galaxies with no SCUBA data are included. The color-color plot using MIPS observations is presented in Figure 6, again showing SLUGS and SINGS galaxies. As in Fig. 5, we discriminate galaxies with good SCUBA observations (diamonds) from those with lower-confidence level measurements (squares) and no SCUBA observations (triangles). The plot shows that SLUGS galaxies are found towards lower values of νF$_\nu$(70μm)/νF$_\nu$(160μm) which is the expected behavior for galaxies with cold dust, though not reaching the levels of NGC 4725 and NGC 2841, which are the most extreme cases in the SINGS sample. On the other hand, the distribution of the νF$_\nu$(24μm)/νF$_\nu$(70μm) colors of the SLUGS sample is similar to that of the SINGS sample.

The data in Table 7 are used to compare the properties of SLUGS galaxies with the Draine et al. (2007) fits for SINGS where the maximum intensity of the starlight (U_{max}) is fixed to 10^6. The SED fits calculated in Section 3.2 suggest that most galaxies in the SLUGS sample have PAH emission, which is further corroborated by the analysis of Bendo et al. (2008). The frequency distribution of the amount of dust contained in small aromatic grains (q_{PAH}) is shown in Figure 7(a). The SLUGS sample is represented by the solid grey histogram while Draine et al. (2007) measurements for SINGS galaxies are outlined as the dotted histogram for the entire sample and the solid line histogram for the SCUBA sub-sample of 17 galaxies. The distribution of aromatic grain indices for SLUGS and the full SINGS is similar in spite of the small number of SLUGS objects. Figure 7(b) shows the distribution of γ, which quantifies the contribution due to starlight re-radiated in photo-dissociation regions relative to the idealized single and constant radiation field U_{min}. The γ distribution for SLUGS has a median value of $\sim 0.6\%$, and the galaxies are all concentrated in a single bin in the histogram; SINGS galaxies have $\gamma \sim 1\%$. This low value of γ for SLUGS has direct implications for the estimate of the average starlight intensity shown in Figure 7(c) which is lower ($< U >_{slugs} \sim 1.3$) than what is measured for SINGS ($< U >_{sings} \sim 2.5$).

Figure 8(a) shows the distribution of total dust masses. SLUGS galaxies have masses ranging from $\sim 10^{6.5}$ $M_\odot$ to $10^{8.5}$ $M_\odot$, with a median of $10^{7.9}$ $M_\odot$, $\sim 3\times$ higher than is measured for the entire sample of SINGS galaxies ($10^{7.4}$ $M_\odot$). However, as noted by Draine et al. (2007), for galaxies without sub-mm data the fitting procedure has to be more constrained otherwise the resulting fits may produce *larger* cold dust masses. However, Draine et al. (2007) find that the mass estimates for $\sim 65\%$ of their sample agree within a factor of 1.5 when fits using and discarding the sub-mm data are compared. Given the uncertainties, the observed difference between SLUGS and SINGS is probably not significant, corroborated by the similar masses of SINGS galaxies with sub-mm data ($10^{7.6}$ $M_\odot$). Figure 8(b) shows the total dust luminosities, which for SLUGS galaxies ($log_{10}L/L_\odot \sim 10.2$) are somewhat higher than for the entire SINGS sample ($log_{10}L/L_\odot \sim 9.7$) (though the distribution is virtually identical to that of the SINGS SCUBA subsample $log_{10}L/L_\odot \sim 10.3$). Differences between the distribution of the dust model parameters were examined using the two-sided Kolmolgorov-Smirnov test (e.g., Press et al. 2002), and the only significant difference between both samples is found for the average starlight field $< U >$ where the probability of both distributions being drawn from the same parent sample is $\lesssim 10^{-5}$.

On average, the SLUGS galaxies have a warm dust component with a median temperature of T_w=54.7±1.7 K and a colder one with T_c= 18.5±1.1 K.

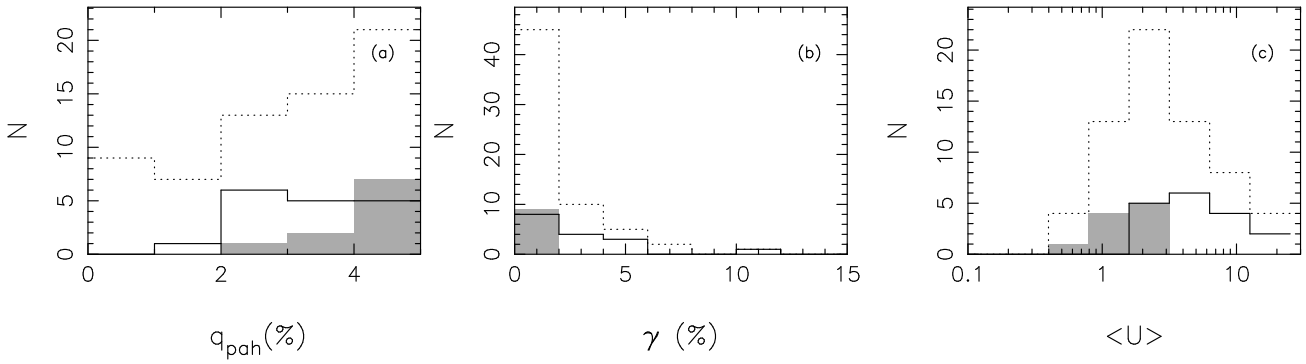

FIG. 7.— Histograms comparing the parameters obtained by fitting the Draine et al. (2007) dust models to the SLUGS galaxies (solid grey histograms), with results tabulated by Draine et al. (2007) for the full SINGS sample (dotted line histogram) and the subsample of 17 galaxies with SCUBA measurements (solid line histogram). This comparison uses the fit parameters obtained by fixing the value of U_{max}. Panel (a) shows the q_{PAH} distribution, which measures the ratio between the dust mass in the form of aromatic grains and the total dust mass. Panel (b) shows the distribution of γ which quantifies the contribution towards the total dust emission from dust located in regions with intense starlight due to very hot stars. Panel (c) shows the average starlight radiation field (<U>) present in the galaxies' interstellar medium.

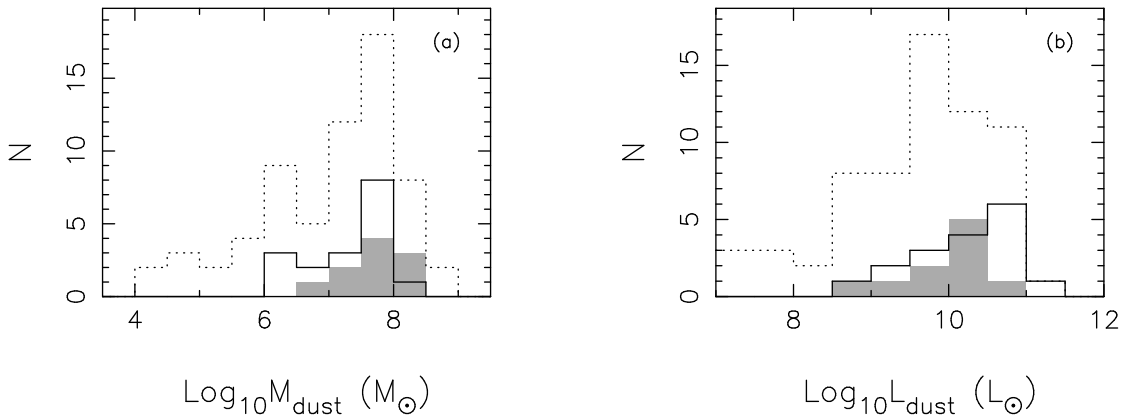

FIG. 8.— Histograms comparing the estimated dust masses (left panel) and luminosities (right panel) for SLUGS (grey histograms), and SINGS galaxies (dotted line histogram). The 17 SINGS galaxies that have SCUBA measurements represented by the solid line histogram. The present sample has marginally higher dust masses than the SINGS sample, though the total dust luminosity is comparable.

Both estimates agree within 2 σ with the results of Vlahakis et al. (2005) who find T_w=47.4±2.4 K and T_c= 20.2±0.5 K respectively. The warm dust temperature is comparable to that measured by Hinz et al. (2007) for UGC 6879, while the the average value we find for the cold dust component is comparable to the Hinz et al. (2006) measurement for the starbursting dwarf galaxy UGC 10445. Similarly to the findings of Vlahakis et al. (2005) and Hinz et al. (2007), most of the dust in these galaxies is cold, with $M_{cold}/M_{warm} \sim 1156\pm658$. The distribution of the ratio between the cold and warm dust components for SLUGS and SINGS is shown in Figure 9. Although there is some overlap in the mass ratios, SINGS galaxies with SCUBA measurements tend to have a smaller contribution due to cold dust with a ratio of 538±305.

The ratio between the total emission integrated from 5–1000 μm, which includes the important contribution due to aromatic emission (e.g., Rieke et al. 2009) and the infrared luminosity in the range 100-1000 μm, which is mostly dominated by the cold dust component, is shown in Fig. 10. SLUGS galaxies are represented by the solid black circles, SINGS galaxies with SCUBA measurements by diamonds or open squares (in the case of low significance level measurements); the triangles represent SINGS galaxies for which the far-IR is not as well constrained because of the absence of SCUBA data. Also shown are the sample of local LIRGs and ULIRGs (squares) and templates for $10^{9.75} \leq L \leq 10^{11}$ $L_\odot$ of Rieke et al. (2009) represented by stars. The SLUGS galaxies populate a region of lower luminosities and with a higher proportion of far-IR emission than the sample of SINGS galaxies with SCUBA measurements. However, it is interesting to note that the constrained Draine & Li (2007) models place many of the SINGS galaxies without SCUBA measurements in roughly the same parameter space as the SLUGS galaxies. The combined SLUGS and SINGS and LIRG/ULIRG samples show a trend where the amount of energy in the far-IR becomes more important as lower luminosities are reached. This trend is also seen in the Rieke et al. (2009) templates.

The new observations reported in this paper suggest that there is a wider variety of sub-mm properties than encompassed by SINGS alone, with a larger fraction

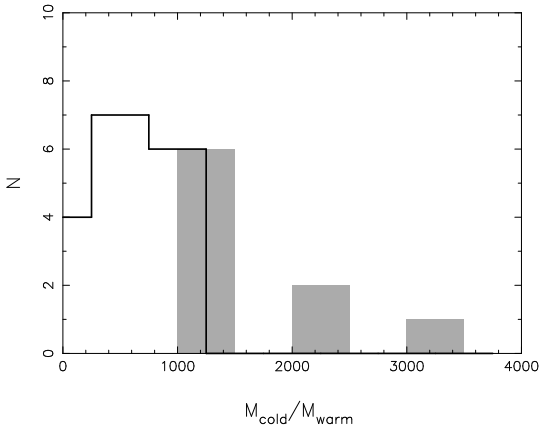

FIG. 9.— Distribution of the mass ratio between cold (T∼19K) and warm (T ∼ 55 K) dust estimated from modified blackbody fits for SINGS and SLUGS galaxies with SCUBA data. The filled histogram represents SLUGS galaxies and the open histogram SINGS galaxies. Although there is significant overlap, SINGS galaxies tend to have smaller mass ratios compared to SLUGS.

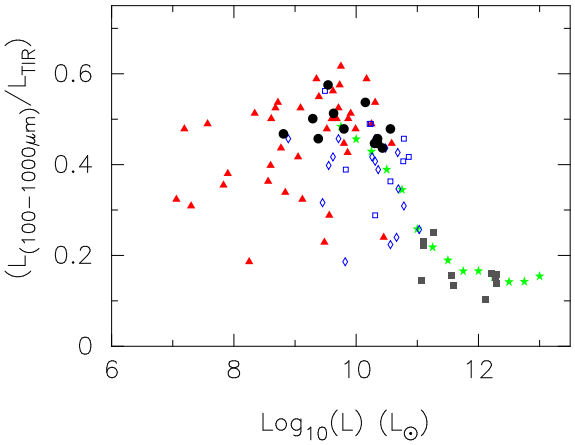

FIG. 10.— Ratio between the luminosity emitted in the far-IR (100-1000 μm) and the total luminosity (5-1000 μm) for SLUGS galaxies (black circles), SINGS galaxies with SCUBA detections (diamonds), those without (triangles); the Rieke et al. (2008) sample of local LIRGs and ULIRGs (solid squares) and the Rieke et al. (2008) templates (stars) covering a range of luminosities from $10^{9.5}$ to 10^{13} $L_\odot$. The local LIRGs and ULIRGs extend to lower values the cold/total emission measured by SINGS and SLUGS. The behavior of the Rieke et al. (2008) templates show that the three samples are complementary. These also suggest that galaxies with lower IR luminosities tend to have a larger contribution of their emission in the far-IR.

of galaxies in the nearby universe presenting significant amounts of dust at temperatures ∼ 18 K. The luminosities of these galaxies (Log($L/L_\odot$) ∼ 10.2) are comparable to some of the least luminous objects detected in the SCUBA Half Degree Extragalactic Survey (SHADES), a blank field survey which scanned several patches of sky (Mortier et al. 2005), in contrast to SLUGS, which targeted optically-detected galaxies. The lower luminosity galaxies in SHADES are characterized as having "cirrus" SEDs (e.g., Clements et al. 2008) and make up ∼ 25 % of the sample of sub-mm galaxies (Clements et al. 2005), suggesting that the local samples are undersampling this type of galaxy.

4. CONCLUSION

We trace the Spectral Energy Distribution for 11 galaxies providing an unbiased sample of sub-mm properties (from the SLUGS selection). We combine new IRAC and MIPS data obtained with the *Spitzer Space Telescope* with existing 850 μm, *IRAS* and near-IR measurements. The new measurements confirm the presence of cold (T∼18K) dust in 10 of these galaxies.

Using fits of Draine & Li (2007) models we show that the contribution due to light reprocessed by photo-dissociation regions is not as important in our sample as it is for SINGS galaxies. The models also suggest that the total IR emission of SLUGS galaxies has a small contribution due to PAH lines emitted in photo-dissociation regions. However the proportion of the total light contributed by the mid-IR emission is smaller than that measured for the SINGS sample. The typical total dust masses obtained using Draine & Li (2007) models are of $10^{7.9} M_\odot$ and dust luminosities are ∼ $10^{10} L_\odot$. The most significant difference between the samples is the lower average intensity of the general radiation field of SLUGS compared to SINGS galaxies. Although the uncertainties are large, SLUGS galaxies show ∼ 2 × larger proportion of cold dust relative to warm than do the SINGS galaxies.

The present data combined with previous observations show that cold dust is present in all types of spirals being the major contributor to their far-infrared luminosity (Tuffs and Popescu 2003). Although the 160 μm data are somewhat shallow, they suggest that qualitatively the scale length distribution of cold dust is at least comparable to what is measured in the mid-infrared and in the visible (e.g., Alton et al. 1998; Davies et al. 1999; Tuffs et al. 2002a, 2002b; Hinz et al. 2006). Since the amount of dust in a galaxy measures the quantity of heavy elements in the ISM, it gives a complementary measure of the average metallicity of galaxy (Dunne et al. 2000). Thus the presence of cold dust suggests that the extended HI in these galaxies is generally not metal-poor.

C.N.A.W. thanks Z. Balog, M. Blaylock and M. Block for their guidance in the reduction of IRAC and MIPS data, T. Lauer for tips on photometry and J. Stansberry for discussions on the calibration of *Spitzer* images. ELF acknowledges the support from the Spitzer Space Telescope Fellowship Program through a contract issued by the Jet Propulsion Laboratory, California Institute of TechnologyJPL/Caltech and National Aeronautics and Space Administration. This work is based in part on observations made with the *Spitzer Space Telescope*, which is operated by the JPL/Caltech under NASA contract 1407. Support for this work was provided by NASA through JPL/Caltech contract 1255094 and by MAG5-12318 from NASA/Goddard to the University of Arizona. This research has made use of NASA's Astrophysics Data System (ADS) and the NASA/Infrared Processing and Analysis Center Extragalactic Database (NED) which is operated by the JPL/Caltech, under contract with NASA. Data also come from the Two Micron All Sky Survey, a joint project of the University of Massachusetts and IPAC/Caltech, funded by NASA and the NSF. We acknowledge the usage of the HyperLeda database (http://leda.univ-lyon1.fr).

REFERENCES

Bell, E. F. 2003, ApJ, 586, 794
Bell, E. F., McIntosh, D., Katz, N., & Weinberg, M. D. 2003, ApJS, 149, 289
Bendo, G. J., et al. 2008, MNRAS, in press, (arXiv 0806.2758)
Bertin, E, & Arnouts, S. 1996, A&AS, 117, 393
Blain, A. W., Chapman, S. C., Smail, I.m & Ivison, R. 2004, ApJ, 611, 52
Busko, I. 1996, in "Astronomical Data Analysis Software and Systems V", eds. G. H. Jacoby & J. Barnes, ASP Conference Series, Vol. 101, 139
Chary, R. R., & Elbaz, D. 2001, ApJ, 556, 562
Clements, D. L., Farrah, D/, Rowan-Robinson, M., Afonso, J., Priddey, R., & Fox, M. 2005, MNRAS, 363, 229
Clements, D. L., et al. 2008, MNRAS, 387, 247
Cutri, R. et al. 2006, "Explanatory Supplement to the 2MASS all Sky Data Release and Extended Mission Products", *http://www.ipac.caltech.edu/2mass/releases/allsky/doc/explsup.html*, Section IV.2
Dale, D. A., Helou, G., Contursi, A., Silbermann, N. A., Kolhatkar, S. 2001, ApJ, 549, 215
Dale, D. A. & Helou, G. 2002, ApJ, 576, 159
Dale, D. A., et al. 2005, ApJ, 633, 857
Dale, D. A., et al. 2007, ApJ, 655, 863
Désert, F. X., Boulanger, F., & Puget, J.-L. 1990, A&A, 237, 215
Devereux, N. A., & Young, J. S., 1990, ApJ, 359, 42
Draine, B. T., & Li, A. 2001, ApJ, 551, 807
Draine, B. T., & Li, A. 2007, ApJ, 657, 810
Draine, B. T., et al. 2007, ApJ, 663, 866
Dunne, L., Eales, S. Edmunds, M, Ivison, R., Alexander, P, & Clemens, D. L. 2000, MNRAS, 315, 115
Elbaz, D., Cezarsky, C. J., Chanial, P., Aussel, H., Franceschini, A., Fadda, D., & Chary, R. R. A&A 384, 848
Engelbracht, C. W., et al. 2007, PASP, 119, 994
Fazio, G. G., et al. 2004, ApJS, 154, 10
Finkbeiner, D. P., Davis, M., & Schlegel, D. J. 1999, ApJ, 524, 867
Galliano, F., Madden, S. C., Jones, A. P., Wilson, C. D., & Bernard, J. -P. 2005, A&A, 434, 867
Giovanini, G., Taylor, G. G., Feretti, L., Cotton, W. D., Lara, L. & Venturi, T. 2005, ApJ, 618, 635
Gordon, K. D., et al. 2005, PASP, 117, 503
Gordon, K. D., et al. 2007, PASP, 119, 1019
Guiderdoni, B., Hivon, E., Bouchet, F. R., & Maffei, B. 1998, MNRAS, 295, 877 Frontiéres), p. 521
Haas, M., Klass, U., & Bianchi, S. 2002, A&A, 385,L23
Haas, M., Lemke, D., Stickel, M. Hippelein, H., Kunkel, M., Herbstmeier, U., & Mattila, K. 1998, A&A, 338, 33
Helou, G. 1986, ApJ, 311, L33
Hippelein, H., Haas, M., Tuffs, R. J., Lemke, D., Stickel, M., Klass, U. & Völk, H. J. 2003, A&A, 407, 137
Hinz, J. L., Misselt, K., Rieke, G. H., Rieke, M. J., Smith, P. S., Gordon, K. D. 2006, ApJ, 651, 874
Hinz, J. L., Rieke, M. J., Rieke, G. H., Willmer, C. N. A., Misselt, K. Engelbracht, C. W., Blaylock, M. & Pickering, T. E. 2007, ApJ, 663, 895
Holland, W. S., et al. 1999, MNRAS, 303, 659
Huchra, J. P., Davis, M., Latham, D. W., & Tonry, J. 1983, ApJS, 52, 89
James, A., Dunne, L., Eales, S., & Edmunds, M. G. 2002, MNRAS, 335, 753
Jarrett, T. H., Chester, T., Cutri, R., Schneider, S., Skrutskie, M., & Huchra, J. P. 2000, AJ, 119, 2498
Jedrzejewski, R. I. 1987, MNRAS, 226, 747
Kessler, M.F., et al. 1996, A&A, 315, L27
Kennicutt, R. C., et al. 2003, PASP, 115, 928
Lagache, G., Dole, H., & Puget, J.-L. 2003, MNRAS, 338, 555
Lagache, G., et al. 2004, ApJS, 154, 112
Lagache, G., Puget, J.-L., Dole, H. 2005, ARAA, 43, 727
Laurent, O., Mirabel, I. F., Charmandaris, V., Gallais, P., Madden, S. C., Sauvage, M., Vigroux, L., & Cezarsky, C. 2000a, A&A, 359, 887
Laurent, O., Mirabel, I. F., Charmandaris, V., Le Floc'h, E., Lutz, D., & Genzel, R. 2000b, in "ISO beyond the peaks: The 2nd ISO workshop on analytical spectroscopy" Eds. A. Salama, M.F.Kessler, K. Leech & B. Schulz, ESA-SP 456, p.249
Le Floc'h, E., et al. 2005, ApJ, 632, 169
Leger, A., & Puget, J.-L. 1984, A&A, 137, L5
Li., A. & Draine, B. T., 2001, ApJ, 554, 778
Li., A. & Draine, B. T., 2002, ApJ, 576, 762
Lonsdale, C. J., & Helou, G. 1987, ApJ, 314, 513
Martin, D. C., et al. 2005, ApJ, 619, L1
Mortier, A. M. J., et al. 2005, MNRAS, 363, 563
Paturel, G., Petit, C., Prugniel, P., Theureau, G., Rousseau, J., Brouty, M., Dubois, P., & Cambrésy, L., 2003, A&A, 412, 45
Peréz-González, P., et al. 2008, ApJ, 675, 234
Popescu, C. C., & Tuffs R. J. 2003, A&A, 410, L21
Press, W. H., Flannery, B. P., Teukolsky, S. A., Vetterling, W. T. 1986, *Numerical Recipes*, (Cambridge: Cambridge Univ. Press)
Puget, J.-L., Abergel, A., Bernard, J.-P., Boulanger, F., Burton, W. B., Désert, F.-X., & Hartmann, D. 1996, A&A, 308, 5
Reach, W. T. et al. 2005, PASP, 117, 978
Rieke, G. H. & Lebofsky, M. J. 1978, ApJ, 222, 37
Rieke, G. H., et al. 2004, ApJS, 154, 25
Rieke, G. H., et al. 2008, AJ, 135, 2245
Rieke, G. H., et al. 2009, ApJ, accepted, arXiv 0810.4150
Sanders, D. B., & Mirabel, I. F. 1996, ARA&A, 34, 749
Sauvage, M., Thuan, T. X. 1992, ApJ, 396, L69
Sauvage, M., Tuffs, R. J., & Popescu, C. C. 2005, Sp. Sci. Rev., 119, 313
Schuster, M. T., Marengo, M. Patten, B. M. 2006, "Observatory Operations: Strategies, Processes, and Systems". Eds: D. R. Silva & R. E. Doxsey, Proceedings of the SPIE, Volume 6270, p. 627020
Serabyn, E., Lis, D. C., Dowell, C. D., Benford, D. J., Hunter, T. R., Trewhella, M., & Moseley, S. H. 1999, in "Astrophysics with Infrared Surveys: A Prelude to SIRTF", Eds. M.D. Bicay, C. A. Beichman, R. M. Cutri, and B. F. Madore, ASPC, 117, 209
Siebenmorgen, R., & Krügel, E. 2007, A&A, 461, 445
Smith, J.-D. T., et al. 2007, ApJ, 656, 770
Stansberry, J., et al. 2007, PASP, 119, 1038
Tuffs, R. J., & Gabriel, C. 2003, A&A, 410, 1075
Tuffs, R. J., & Popescu, C. C. 2005, in "The Spectral Energy Distribution of Gas-Rich Galaxies: Confronting Models with Data", (eds. C.C. Popescu & R. J. Tuffs), (New York: AIP), p. 344

Vlahakis, C., Dunne, L. & Eales, S. 2005, MNRAS, 364, 1253
Weingartner, & Draine, B. 2001a, ApJ, 548, 296
Weingartner, & Draine, B. 2001b, ApJS, 134, 263
Wen, X.-Q., Wu, H., Cao, C., Xia, X.-Y., 2007, ChJAA, 7, 187